PIP_2 corrects cerebral blood flow deficits in small vessel disease by rescuing capillary Kir2.1 activity

Fabrice Dabertrand[a,b,c,1,2], Osama F. Harraz[a,d,1], Masayo Koide[a,d], Thomas A. Longden[a,3], Amanda C. Rosehart[a,b], David C. Hill-Eubanks[a], Anne Joutel[a,e,f], and Mark T. Nelson[a,d,g,2]

[a]Department of Pharmacology, Larner College of Medicine, University of Vermont, Burlington, VT 05405; [b]Department of Anesthesiology, University of Colorado Anschutz Medical Campus, Aurora, CO 80045; [c]Department of Pharmacology, University of Colorado Anschutz Medical Campus, Aurora, CO 80045; [d]Vermont Center for Cardiovascular and Brain Health, University of Vermont, Burlington, VT 05405; [e]Institute of Psychiatry and Neurosciences of Paris, INSERM UMR1266, University of Paris, F-75014 Paris, France; [f]Psychiatrie et Neurosciences, Groupe Hospitalier Universitaire Paris, F-75014 Paris, France; and [g]Division of Cardiovascular Sciences, University of Manchester, Manchester M13 9PL, United Kingdom

Contributed by Mark T. Nelson, March 16, 2021 (sent for review December 22, 2020; reviewed by Scott Earley and David Kleinfeld)

Cerebral small vessel diseases (SVDs) are a central link between stroke and dementia—two comorbidities without specific treatments. Despite the emerging consensus that SVDs are initiated in the endothelium, the early mechanisms remain largely unknown. Deficits in on-demand delivery of blood to active brain regions (functional hyperemia) are early manifestations of the underlying pathogenesis. The capillary endothelial cell strong inward-rectifier K^+ channel Kir2.1, which senses neuronal activity and initiates a propagating electrical signal that dilates upstream arterioles, is a cornerstone of functional hyperemia. Here, using a genetic SVD mouse model, we show that impaired functional hyperemia is caused by diminished Kir2.1 channel activity. We link Kir2.1 deactivation to depletion of phosphatidylinositol 4,5-bisphosphate (PIP_2), a membrane phospholipid essential for Kir2.1 activity. Systemic injection of soluble PIP_2 rapidly restored functional hyperemia in SVD mice, suggesting a possible strategy for rescuing functional hyperemia in brain disorders in which blood flow is disturbed.

functional hyperemia | cerebral small vessel diseases | CADASIL | potassium channel | PIP_2

Cerebral small vessel diseases (SVDs), a seemingly intractable ensemble of genetic and sporadic diseases that progress silently for years before becoming clinically symptomatic, have emerged as a central link between stroke and dementia—two comorbidities that rank among the most pressing human health issues (1, 2). SVDs are responsible for more than 25% of ischemic strokes (1) and are the leading cause of age-related cognitive decline and disability, accounting for more than 40% of dementia cases (1, 3). Despite the enormous impact of SVDs on human health, the disease processes and key biological mechanisms underlying these disorders remain largely unknown. Notably, there are no specific treatments for sporadic or genetic SVDs (4).

In the healthy brain, cerebral blood flow (CBF) is controlled so as to meet the changing demands of active neurons. This activity-dependent blood-delivery process (functional hyperemia) is rapidly and precisely controlled through a number of molecular mechanisms collectively termed "neurovascular coupling." We demonstrated that brain capillaries act as a neural activity-sensing network, showing that brain capillary endothelial cells (cECs) are capable of initiating an electrical (hyperpolarizing) signal in response to neural activity that propagates retrogradely to dilate upstream feeding arterioles, thereby increasing local blood flow. We have further established that extracellular K^+—a byproduct of every neuronal action potential—is the critical mediator of this process and have identified the cEC strong inward-rectifier K^+ channel, Kir2.1, as the target of K^+ ions (5–7). Notably, we have further shown that phosphatidylinositol 4,5-bisphosphate (PIP_2), a minor inner leaflet phospholipid, is an important physiological regulator of cEC Kir2.1 channels (8–10), a finding in accord with previous studies demonstrating the requirement of PIP_2 for channel activity (11, 12).

Cerebral autosomal dominant arteriopathy with subcortical infarcts and leukoencephalopathy (CADASIL), caused by highly stereotyped mutations in the extracellular domain of the NOTCH3 receptor, is the most common monogenic inherited form of SVD and a model for more frequent sporadic forms (2, 3). We recently demonstrated that defective functional hyperemia is an early disturbance in the *TgNotch3*^{R169C} mouse model of CADASIL (13), which overexpresses a mutation identified in humans (14). Notably, CADASIL patients exhibit deficits in functional hyperemia long before evidence of significant disability or cognitive decline (15). Our recent studies using the *TgNotch3*^{R169C} mouse model (hereafter, SVD mice) implicate altered extracellular matrix dynamics in this disease. Specifically, these studies showed that the matrix metalloproteinase inhibitor TIMP3, which accumulates in NOTCH3 extracellular domain (NOTCH3^{ECD}) deposits surrounding vascular smooth muscle cells (SMCs) and pericytes, suppresses the activity of the matrix metalloproteinase ADAM17, inhibiting shedding of the epidermal growth factor receptor

Significance

Years before the emergence of infarctions or significant cognitive decline, patients with cerebral small vessel disease (SVD) show a deterioration in the ability of the brain to augment blood flow locally in response to increases in neuronal activity (functional hyperemia). Using a well-characterized genetic mouse model of a hereditary form of SVD, we determined the molecular defect at play in capillary endothelial cells. We found that SVD is associated with reduced synthesis of the phospholipid PIP_2, which prevents the Kir2.1 channel-initiated capillary-to-arteriole electrical signaling that supports vasodilatory responses during functional hyperemia. We further show that systemic injection of exogenous PIP_2 is sufficient to rescue this deficit in SVD mice, restoring adequate cerebral blood flow in response to neuronal activation.

Author contributions: F.D., O.F.H., and M.T.N. designed research; F.D., O.F.H., M.K., T.A.L., and A.C.R. performed research; F.D., O.F.H., M.K., T.A.L., and A.C.R. analyzed data; and F.D., O.F.H., D.C.H.-E., A.J., and M.T.N. wrote the paper.

Reviewers: S.E., University of Nevada, Reno School of Medicine; and D.K., University of California at San Diego.

Competing interest statement: Exogenous PIP_2 administration was submitted as patent number 62/823,378 titled "Methods to promote cerebral blood flow in the brain" on 25 March 2019.

[1]F.D. and O.F.H. contributed equally to this work.

[2]To whom correspondence may be addressed. Email: fabrice.dabertrand@cuanschutz.edu or Mark.Nelson@uvm.edu.

[3]Present address: Department of Physiology, University of Maryland School of Medicine, Baltimore, MD 21201.

This article contains supporting information online at https://www.pnas.org/lookup/suppl/doi:10.1073/pnas.2025998118/-/DCSupplemental.

Published April 19, 2021.

(EGFR) ligand heparin-binding EGF-like growth factor (HB-EGF), thereby decreasing EGFR activity (13, 16–19). One direct consequence of this decreased ADAM17/HB-EGF/EGFR signaling is a reduction in functional hyperemia (13). However, the basis of this deficit is not known. Here, we found that a mechanism—Kir2.1 channel down-regulation in cECs—operates to abrogate capillary-to-arteriole electrical signaling and cause functional hyperemia deficits.

Results

Propagated Electrical Signaling Is Abolished and the Kir Channel Component of Functional Hyperemia Is Lost in SVD. Our previous report that cEC Kir2.1-mediated, propagating electrical (hyperpolarizing) signaling is a major contributor to the functional hyperemic response (5, 8), taken together with our demonstration that whisker stimulation-induced functional hyperemia is substantially reduced in SVD mice (13, 14), suggested the possibility of impaired electrical signaling in this model. We hypothesized that pathogenic accumulation of TIMP3 and subsequent inhibition of the EGFR pathway would also manifest at the capillary level (Fig. 1*A*). To investigate this, we tested whether focal application (pressure ejection) of a solution containing an elevated K^+ concentration (10 mM K^+ vs. a basal level of 3 mM) (*SI Appendix*, Table S1) onto capillary extremities was capable of causing dilation of the attached upstream arteriolar segment in our pressurized (40 mmHg), ex vivo capillary-parenchymal arteriole (CaPA) preparation (Fig. 1*B* and *SI Appendix*, Table S2 and Fig. S1) (5, 8). K^+ stimulation of capillary extremities in CaPA preparations from *TgNotch3*^{WT} mice (hereafter, wild-type [WT] mice) induced robust dilation of the upstream arteriole segment (Fig. 1 *C* and *D*). In stark contrast, the same K^+ stimulus failed to evoke a dilatory response in CaPA preparations from SVD mice, indicating that capillary-to-arteriole electrical signaling is abolished in SVD (Fig. 1 *C* and *D* and Movie S1). Interestingly, arterioles from SVD mice retained their responsiveness to K^+ stimulation, as evidenced by the similar, robust response to 10 mM K^+, directly applied onto the upstream arteriole, in CaPA preparations from both WT and SVD mice (Fig. 1 *B–D* and Movie S1) (17). Collectively, these results indicate that the molecular defect responsible for the loss of electrical signaling in SVD mice is restricted to capillaries.

We also previously showed that pressure-induced constriction (myogenic tone) is impaired in arterioles from SVD mice, reflecting up-regulation of the voltage-dependent potassium (K^+) channel, $K_V1.5$, in arteriolar SMCs (13, 14, 17, 19, 20). As expected, arterioles from SVD mice developed less myogenic tone (21.9 ± 1.6%) than control arterioles (39.9 ± 1.3%) upon elevation of intravascular pressure to 40 mmHg (*SI Appendix*, Table S2). To test whether this deficit contributes to impaired functional hyperemia, we normalized tone in SVD arterioles by partially inhibiting K_V1 channels with 4-aminopyridine (4-AP) (1 mM) and then measured the effects of capillary-applied K^+ on SVD arteriole dilation (*SI Appendix*, Fig. S2 *A* and *B*) (17, 19). Even at the same level of myogenic tone, capillary-applied K^+ (10 mM) failed to induce a change in arteriolar diameter (*SI Appendix*, Fig. S2*C*), suggesting that functional hyperemia deficits are unrelated to $K_V1.5$ up-regulation.

To confirm these results in vivo, we tested dilation of upstream arterioles in response to direct stimulation of brain capillaries with K^+ by recording capillary red blood cell (RBC) flux through a cranial window using two-photon laser-scanning microscopy. Fluorescein isothiocyanate (FITC)-labeled dextran was injected into the circulation of anesthetized mice to visualize the parenchymal microcirculation and enable RBC tracking (Fig. 1*E*). To stimulate brain capillaries, we positioned a micropipette (tip diameter, 1 to 2 μm) containing a 10 mM K^+ solution adjacent to a capillary segment and raised local K^+ by pressure ejection (8 ± 2 pounds per square inch [psi]) for 300 ms. In control WT mice, this stimulus evoked a rapid increase in capillary RBC flux (Δ = 11.1 ± 2.3 RBCs/s). In keeping with results obtained ex vivo, elevation of external K^+ in vivo had no effect on RBC flux in the brain microvasculature of SVD mice (Fig. 1 *F–H*). Collectively, these results demonstrate that capillary-to-arteriole electrical signaling is lost in the SVD model, ex vivo and in vivo (Fig. 1).

Kir2.1 Channel Down-Regulation in cECs Underlies Deficits in Electrical Signaling and Functional Hyperemia in SVD. To explore the effects of the *Notch3*^{R169C} mutation on capillary-mediated electrical signaling and functional hyperemia, we measured whisker stimulation-evoked CBF responses in the somatosensory cortex through a cranial window in SVD mice using laser Doppler flowmetry (LDF); WT mice were used as controls (Fig. 2 *A–C*). Consistent with our previous reports (13, 14), whisker stimulation-evoked CBF increases were markedly blunted in SVD mice (15.1 ± 1.0%) compared with WT mice (26.0 ± 2.2%) (Fig. 2 *B* and *C*). To isolate the electrical (Kir-dependent) component of functional hyperemia, we superfused the cortex with 100 μM barium (Ba^{2+}), a pore blocker that potently inhibits Kir2 channels (*SI Appendix*, Table S1) (21, 22). In WT mice, 76.9 ± 4.0% of the hyperemic response was Kir-dependent (i.e., Ba^{2+} sensitive) (Fig. 2 *B* and *C*), consistent with our previous measurements (5). In sharp contrast, and consistent with our ex vivo results obtained using the CaPA preparation, the majority of this Kir-dependent component of functional hyperemia was absent in SVD mice (Fig. 2 *B* and *C*). Taken together with the observation that the molecular defect responsible for the loss of electrical signaling in CASASIL mice is restricted to capillaries, these findings suggest the involvement of Kir 2.1 channels in cECs.

To directly test the possibility that a decrease in functional cEC Kir2.1 channels—the molecular lynchpin of the electrical-based neurovascular coupling mechanism—underlies the observed loss of K^+ responsiveness in capillaries from SVD mice, we measured Kir2.1 currents in freshly isolated brain cECs from WT and SVD mice (Fig. 2 *D* and *E*). Currents induced by a 300-ms voltage-ramp (−140 to +40 mV, from a holding potential of −50 mV) were recorded in the perforated whole-cell configuration using a bath solution containing 60 mM K^+, included to increase Kir2.1 current amplitude. Currents recorded in cECs from WT mice exhibited a large inward component negative to the K^+ equilibrium potential (E_K) (−23 mV at 60 mM K^+) and a strongly rectifying component at potentials depolarized relative to E_K (Fig. 2*D*), properties characteristic of Kir2 channels. Notably, at −140 mV, the maximal current density in cECs from SVD mice (−8.4 ± 1.5 pA/pF) was lower than that in cECs from WT controls (−16.5 ± 2.8 pA/pF) (Fig. 2 *D* and *E*), a decrease that we have previously shown is of sufficient magnitude to abolish capillary-to-arteriole electrical signaling (8). In contrast, Kir2.1 current densities in arteriolar ECs and SMCs from SVD mice were unchanged compared with those from WT mice (*SI Appendix*, Fig. S3), supporting the observed retention of dilatory responses to direct arteriolar application of K^+ and further confirming that Kir2.1 channel function is compromised specifically in ECs in the capillary bed.

The TIMP3/ADAM17/HB-EGF/EGFR Pathway Is Involved in the Reduction of cEC Kir2.1 Channel Activity. We next sought to investigate whether alterations in the TIMP3/ADAM17/HB-EGF/EGFR pathway, which impair arteriolar myogenic responses in SVD mice (13), are also involved in cEC Kir channel down-regulation. Perivascular accumulation of TIMP3, which inhibits ADAM17-mediated HB-EGF shedding, is the pathological process underlying EGFR pathway inhibition and impaired in vivo cerebral hemodynamics in SVD mice (Fig. 3*A*) (13, 16–18). Thus, we tested whether bypassing TIMP3-mediated inhibition of ADAM17 with soluble ADAM17 (sADAM17) was capable of normalizing capillary-to-arteriole electrical signaling in SVD mice. Indeed, we found that bath application of enzymatically active sADAM17 (3.2 nM)

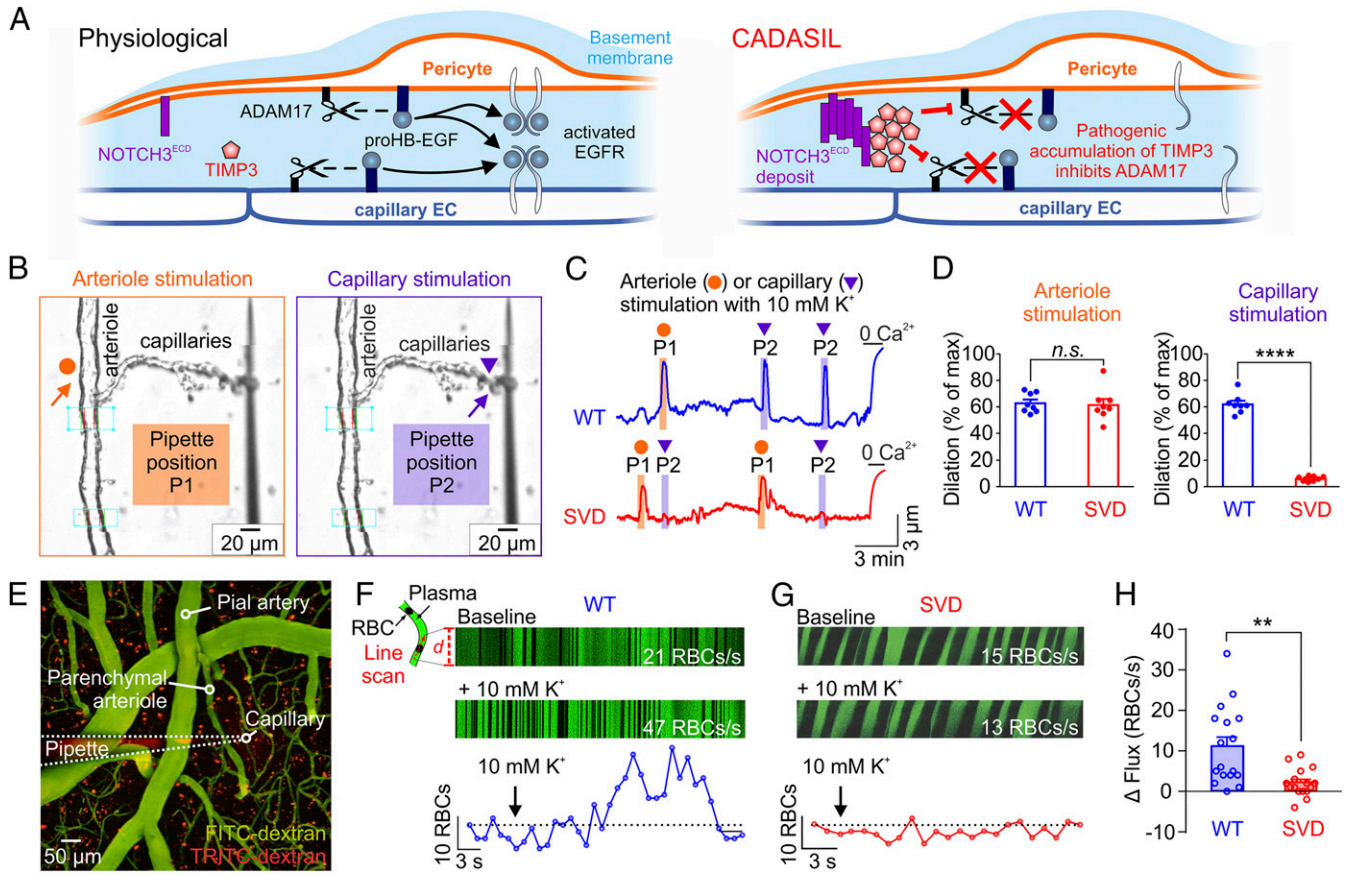

Fig. 1. Capillary-to-arteriole electrical signaling during functional hyperemia is abrogated in SVD. (*A*) Proposed mechanism for pathogenic blunting of EGFR activation by accumulation of TIMP3 in CADASIL at the capillary level. (*B*) Pipette positions for arteriole stimulation (*Left*, orange arrow) and capillary stimulation (*Right*, purple arrow) in CaPA preparations. (*C*) Representative traces of arteriolar diameter showing effects of pressure ejection of 10 mM K^+ onto capillaries (P2, purple triangle) on the diameter of upstream arteriolar segments in control preparations from WT and SVD mice. (*D*) Summary data from 8 WT and 8 SVD mice (*n.s.*, not significant; ****$P < 0.0001$, unpaired Student's *t* test). (*E*) Micrograph displaying a micropipette containing 10 mM K^+ and TRITC-dextran (red) in close apposition to a capillary (FITC-dextran, green) in SVD mice. RBC flux induced by local ejection of K^+ onto the capillary was measured by high-frequency line scanning. (*F* and *G*) (*Top Panels*) Raw recordings showing RBC flux at baseline and after application of 10 mM K^+ onto a capillary in WT (*F*) and SVD (*G*) mice. RBCs appear as black streaks in plasma (green). *x* axis, time; *y* axis, scanned capillary distance, *d*. (*Bottom*) Full trace from raw recordings shown above. (*H*) Summary data showing that K^+-evoked hyperemia is crippled in SVD mice (n = 16–17 experiments in seven to eight mice; **$P < 0.01$, unpaired Student's *t* test).

restored capillary-mediated, K^+-induced upstream arteriolar dilation over time in CaPA preparations from SVD mice (Fig. 3*B*). As anticipated (13), this maneuver increased arteriolar myogenic tone, reflecting the ability of sADAM17 to promote HB-EGF shedding and subsequent EGFR-dependent down-regulation of $K_V1.5$ channels in arteriolar SMCs (Fig. 3*B*). Blocking EGFRs with the antagonist AG1478 (2 µM) prevented both the constriction to sADAM17 and the ability of sADAM17 to restore retrograde vasodilation in SVD (Fig. 3 *C* and *D*), confirming that these effects of sADAM17 are dependent on EGFR activity.

As an alternative approach for testing the centrality of TIMP3 in Kir2.1 down-regulation and attendant loss of electrical signaling in SVD mice, we applied recombinant TIMP3 (8 nM) to CaPA preparations from WT mice and assessed capillary-to-arteriole electrical signaling. Because bath-applied TIMP3 caused dilation of the attached arteriole segment (*SI Appendix*, Fig. S4), presumably through up-regulation of $K_V1.5$ channels in arteriolar SMCs (13), we performed these experiments in the presence of 4-AP, added to normalize tone. Under these conditions, TIMP3 gradually reduced, and ultimately abolished, the arteriolar dilatory response to capillary-applied K^+ (10 mM) in CaPA preparations from WT mice (Fig. 3 *E* and *F*).

Genetic reduction of *Timp3* expression in the context of the *Notch3*^{R169C} mutation (*TgNotch3*^{R169C};*Timp3*$^{+/-}$ mice), a complementary double-mutant approach that restores normal hyperemic responses to whisker stimulation (13), also restored capillary-mediated, K^+-induced, Ba^{2+}-sensitive upstream dilation in CaPA preparations (Fig. 3 *G* and *H*). Notably, whisker stimulation-induced increases in CBF were normalized in *TgNotch3*^{R169C};*Timp3*$^{+/-}$ mice, and the Ba^{2+}-sensitive component of the hyperemic response was restored to WT levels (Fig. 3*I*). Kir2.1 currents were also significantly larger (essentially identical to WT levels) in isolated brain cECs from *TgNotch3*^{R169C};*Timp3*$^{+/-}$ mice compared with those from SVD *TgNotch3*^{R169C} mice (Fig. 3 *J* and *K*). Collectively, these data support a pathomechanism in which accumulated extracellular TIMP3 inhibits ADAM17 sheddase activity to reduce cEC Kir2.1 activity.

Finally, we tested the effect of HB-EGF (30 ng/mL), which we previously showed restores myogenic tone through an EGFR-dependent process (17, 19). Application of HB-EGF caused a rapid (within 10 min), sustained constriction in arteriolar segments in SVD CaPA preparations (Fig. 4*A*), consistent with enhanced EGFR-mediated $K_V1.5$ channel down-regulation in arteriolar SMCs. Interestingly, ~15 min following application of HB-EGF, arteriolar dilatory responses to capillary stimulation with 10 mM K^+ (tested every 5 min) emerged, and the amplitude of these

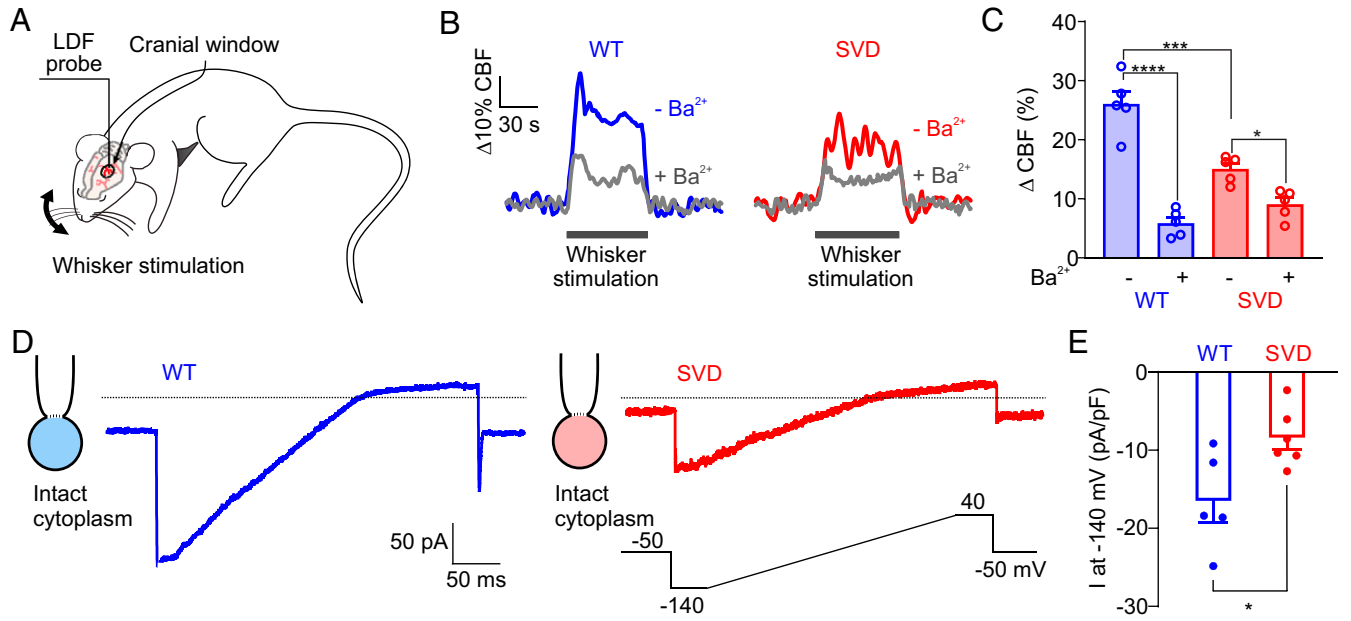

Fig. 2. Kir2.1 channel down-regulation underlies deficits in capillary-to-arteriole electrical signaling in SVD. (*A*) Whisker stimulation experimental scheme. (*B*) Representative traces showing whisker stimulation-induced changes in CBF in control WT (blue) and SVD (red) mice in the presence (gray traces) and absence of Ba^{2+} (100 μM). (*C*) Summary data from five WT and five SVD mice (*$P < 0.05$, ***$P < 0.001$, ****$P < 0.0001$, repeated-measures two-way ANOVA). (*D*) Representative traces of Kir2.1 currents in cECs from WT (blue) or SVD (red) mice, recorded in the perforated-patch configuration. (*E*) Summary data showing Kir2.1 currents (n = 5–6 cECs from three mice per group; *$P < 0.05$, unpaired Student's t test).

responses gradually increased to a maximal value after 35 min of exposure (Fig. 4 *A* and *D*). The slower time course of the restoration of K^+-induced dilations to HB-EGF compared with the constriction to HB-EGF may reflect the requirement for achieving a critical Kir2.1 density sufficient to sustain K^+-induced dilations (8, 9). This HB-EGF–induced restoration of the dilatory response to 10 mM K^+ was prevented by the EGFR antagonist, AG1478, or genetic deletion of Kir2.1 channel specifically in the endothelium (EC-Kir2.1$^{-/-}$ mice) (Fig. 4 *B–D*). Consistent with its ability to rescue upstream dilatory responses to capillary-applied K^+, HB-EGF restored Kir2.1 channel currents in cECs from SVD mice without affecting currents in cECs from WT mice (Fig. 4 *E* and *F*). When applied in vivo, HB-EGF (30 ng/mL, 40-min cortical superfusion) rescued CBF responses to whisker stimulation in SVD mice (Fig. 4 *G* and *H*) as we previously reported (13). This effect was inhibited by Ba^{2+}, implying that functional hyperemia is restored by rescuing cEC Kir2.1 functionality (Fig. 4*H*). Together, these findings indicate that excess TIMP3 impairs functional hyperemia in SVD mice by suppressing the ADAM17/HB-EGF/EGFR pathway at the capillary level, which leads to a reduction in cEC Kir channel activity.

PIP_2 Depletion Is Responsible for the Reduction in Kir2.1 Currents, K^+-Induced Dilations, and Functional Hyperemia in SVD. PIP_2 binding to Kir2 channels is an absolute requirement for the activity of these channels (11, 12). We recently showed that cEC Kir2.1 channels can be silenced by depletion of PIP_2, either experimentally by dialysis in patch-clamp studies or physiologically through G_q protein-coupled receptor (G_qPCR) signaling-mediated hydrolysis (8). This suggests the possibility that Kir2.1 channels are inactivated in SVD through a reduction in PIP_2. We tested this hypothesis electrophysiologically at the single-cell level in the conventional whole-cell configuration, which allows intracellular content to be controlled by manipulating the composition of the pipet solution. Using a patch pipette containing an intracellular solution lacking ATP and PIP_2, we found that Kir2.1 channel current density in cECs from SVD mice (−5.2 ± 1.1 pA/pF), measured within 5 min of gaining access to the cell's interior, was lower than that in cECs from WT mice (−15.9 ± 3.3 pA/pF) (Fig. 5 *A* and *B*). This reduction is similar to that measured in the cytoplasm-intact, perforated-patch configuration, implying that cECs from SVD mice are deficient for ATP or PIP_2. Consistent with this, inclusion of the synthetic PIP_2 analog, diC8-PIP_2, in the patch pipette (without ATP) restored cEC Kir2.1 currents within 30 s of breaking into the cell and had no effect on currents in WT cells (*SI Appendix*, Fig. S5). Incubation of cells with externally applied diC16-PIP_2 (10 μM), a longer-chain PIP_2 analog, for 20 min similarly restored Kir2.1 currents (measured in the conventional whole-cell configuration) in cECs from SVD mice (Fig. 5 *C* and *D*).

We tested the ability of PIP_2 to rescue Kir-mediated dilation ex vivo (CaPA preparation) and in vivo. Exogenous application of diC16-PIP_2 (10 μM) to CaPA preparations from SVD mice fully restored K^+-induced dilations within 20 min (Fig. 5 *E* and *F* and Movie S2). As expected, 30 μM Ba^{2+} abolished this effect (Fig. 5 *E* and *G*). Moreover, diC16-PIP_2 did not restore dilations to capillary-applied K^+ (10 mM) in CaPA preparations from EC-Kir2.1$^{-/-}$ mice (Fig. 5*F*), confirming that the restorative effect of diC16-PIP_2 on K^+-induced dilations is dependent on EC Kir2.1 channels. Importantly, bath-applied PIP_2 did not affect myogenic tone in isolated, pressurized intracerebral arterioles from WT or SVD mice (*SI Appendix*, Fig. S6), reinforcing the conclusion that, although defects in the myogenic response and Kir-induced dilation are both attributable to dysregulation of the TIMP3/ADAM17/HB-EGF axis, the molecular mechanisms in the two cases differ (*SI Appendix*, Fig. S7). Using a soluble form of PIP_2 labeled with a 4,4-difluoro-4-bora-3a,4a-diaza-s-indacene (BODIPY) fluorophore, we confirmed that exogenous PIP_2 is taken up by cECs in the ex vivo CaPA preparation and further demonstrated the mobility of fluorescently labeled PIP_2 in the plasma membrane of these cells using a fluorescence recovery after photobleaching (FRAP) protocol (*SI Appendix*, Fig. S8). Finally, we found that systemic administration of diC16-PIP_2 (0.5 mg/kg) via a femoral artery canula improved functional hyperemia in SVD model

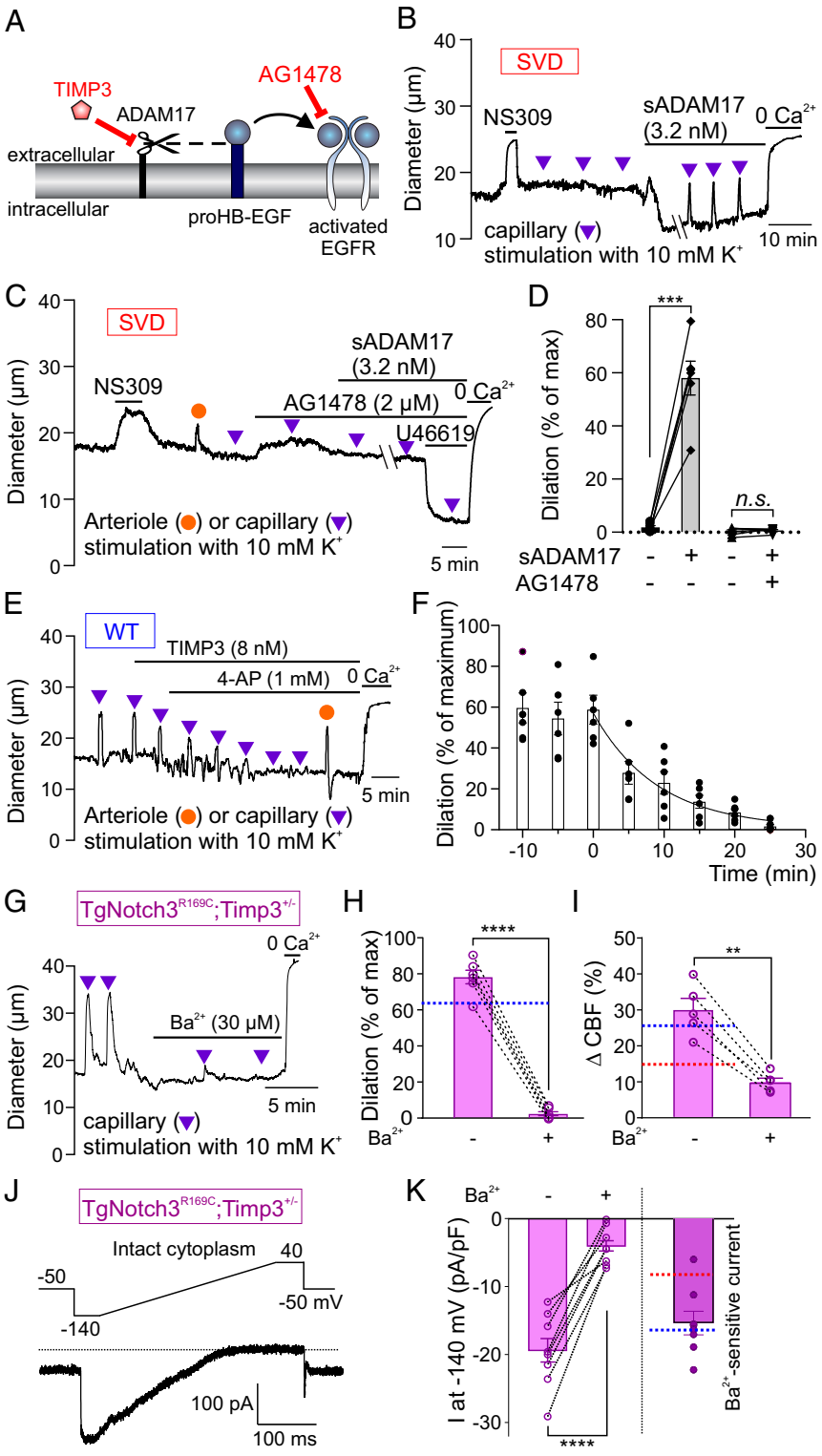

Fig. 3. Pathogenic accumulation of TIMP3 reduces Kir2.1 currents and K^+-induced dilations in SVD. (*A*) ADAM17/HB-EGF/EGFR signaling axis. TIMP3 inhibits ADAM17-mediated cleavage of proHB-EGF (black dashed line) and subsequent EGFR activation by HB-EGF (black arrow). (*B*) Arteriole diameter trace in a CaPA preparation from an SVD mouse showing myogenic tone and arteriolar dilation induced by capillary stimulation with 10 mM K^+ in the presence of bath-applied sADAM17. (*C*) Trace showing block of sADAM17 effects by the EGFR antagonist AG1478. (*D*) Summary data from two groups of six SVD mice showing arteriolar dilation induced by capillary stimulation with 10 mM K^+ (*n.s.*, not significant; ***$P < 0.001$, paired Student's *t* test). (*E*) Arteriole diameter trace showing effects of bath-applied TIMP3 on capillary-to-arteriole electrical signaling in WT CaPA preparation. (*F*) Summary data for *E* from six WT animals. (*G*) Arteriolar diameter trace in a CaPA preparation showing rescue of capillary-to-arteriole electrical signaling by genetic reduction of TIMP3 expression in SVD mice. (*H*) Summary data from six *TgNotch3^{R169C};Timp3$^{+/-}$* mice showing inhibitory effect of 100 µM Ba^{2+} on K^+ (10 mM)-induced dilation (****$P < 0.0001$, paired Student's *t* test). Dotted blue line indicates dilation observed in a WT CaPA preparation, as in Fig. 1*C*. (*I*) Whisker stimulation-induced CBF increases in five *TgNotch3^{R169C};Timp3$^{+/-}$* mice in the absence and presence of 100 µM Ba^{2+} (**$P < 0.01$, paired Student's *t* test). Dotted lines indicate whisker stimulation–induced CBF changes in SVD (red) and WT (blue) mice in the absence of Ba^{2+}, as in Fig. 2*C*. (*J*) Ba^{2+}-sensitive Kir2.1 current in a *TgNotch3^{R169C};Timp3$^{+/-}$* cEC, recorded in the perforated patch-clamp configuration. (*K*) Summary data showing currents recorded from *TgNotch3^{R169C};Timp3$^{+/-}$* cECs in the absence and presence of 100 µM Ba^{2+} ($n = 8$ cECs from two mice; ****$P <$ 0.0001, paired Student's *t* test). (*Right*) Ba^{2+}-sensitive Kir2.1 current. Dotted lines indicate current density observed in SVD (red) and WT (blue) cECs as in Fig. 2*E*.

animals by 45.6 ± 10.9%, measured as an increase in the CBF response to whisker stimulation, without affecting heart rate (baseline, 558 ± 25 beats per minute [bpm]; +PIP_2, 563 ± 28 bpm) or blood pressure (baseline, 114.4 ± 7.2 mmHg; +PIP_2, 113.9 ± 7.4 mmHg); this effect was abolished in the presence of the Kir2.1 inhibitor, Ba^{2+} (100 µM) (Fig. 5 *H* and *I* and *SI Appendix*, Table S3). Collectively, these results indicate that crippled K^+-induced dilation and deficits in functional hyperemia in SVD are attributable to a reduction in cEC Kir2.1 channel function caused by insufficient levels of PIP_2 and that exogenous application of PIP_2 is capable of rescuing these deficits.

Loss of PIP_2 in SVD Reflects Diminished PIP_2 Synthesis. We have previously shown that G_qPCR stimulation deactivates cEC Kir2.1 currents through breakdown of PIP_2 and that clamping intracellular ATP at a low concentration by dialyzing cECs with 0.1 mM

ATP leads to a progressive loss of Kir2.1 channel function that is prevented by inclusion of PIP_2 in the pipette (8). We thus tested whether constitutive G_qPCR activation is the underlying cause of the loss of PIP_2. Kir2.1 currents in cECs from SVD mice, measured using the cytoplasm-intact, perforated-patch configuration, were not restored by exogenous application of the $G\alpha_{q/11}$ inhibitor YM-254890 or the phospholipase C inhibitor U73122 (Fig. 6*A*), implying that enhanced G_qPCR/PLC signaling-dependent PIP_2 hydrolysis is not responsible for PIP_2 depletion and subsequently diminished cEC Kir2.1 channel activity in SVD mice. We thus examined whether the observed decrease in Kir2.1 channel activity is attributable to impaired PIP_2 synthesis, which is mediated by the sequential actions of phosphatidylinositol 4-kinase (PI4K) and phosphatidylinositol 4-phosphate 5-kinase (PIP5K) (23). Notably, although different isoforms/splice variants of PI4K and PIP5K may have differing ATP requirements, both of these enzymes are dependent on relatively high levels of Mg-ATP. In particular, the Michaelis constant of PI4K for ATP is ~0.4 to 1 mM (24–27). We found that increasing ATP in the pipette to 1 mM increased Kir2.1 currents in cECs from SVD mice to WT levels within seconds of breaking into the cell's interior (Fig. 6 *B* and *C*), suggesting that the deficit in functional hyperemia in SVD mice is a result of compromised PIP_2 synthesis in cECs. Notably, direct measurement of ATP in cECs using both a luciferase-based approach and a live-cell ATP dye (ATP-Red1) (*Materials and Methods*) revealed that ATP levels in brain cECs from SVD mice were lower than those from WT mice (Fig. 6 *D–F*). Strikingly, incubation of SVD cECs with HB-EGF for 30 min restored intracellular ATP to WT levels (Fig. 6 *G–I*). Moreover, Kir2.1 currents (measured in the conventional whole-cell configuration) were unaffected by HB-EGF in cells in which intracellular ATP was clamped at a low level by inclusion of 0.1 mM ATP in the pipette solution (Fig. 6*J*). These results collectively support the conclusion that suppressed ADAM17-mediated HB-EGF shedding and diminished EGFR signaling in SVD due to increased TIMP3 activity are responsible for the decreased levels of intracellular ATP, which, in turn, contribute to decreased PIP_2 synthesis, suppression of Kir2.1 channel activity, and subsequent deficits in K^+-induced dilation and functional hyperemia (Fig. 7 and *SI Appendix*, Fig. S7).

Discussion

The well-characterized *TgNotch3*^{R169C} mouse model used in the present study has proved invaluable for understanding pathomechanisms in cerebral SVDs. Using this model to explore the basis of early functional hyperemia deficits, we found that cEC-mediated electrical signaling was completely absent in the brains of SVD mice. Consistent with this, Kir2.1 currents were decreased by approximately one-half specifically in cECs, but not in arteriolar ECs or SMCs, from SVD mice. We further found that these deficits are attributable to the pathological accumulation of TIMP3 protein, which inhibits the ADAM17/HB-EGF/EGFR signaling axis. The resulting decrease in EGFR pathway activity disturbs cEC metabolism, decreasing the cytosolic ATP concentration and thereby impairing PIP_2 synthesis and reducing the available plasma membrane pool of PIP_2, which we previously demonstrated is critical for sustaining Kir2.1 channel-mediated electrical signaling (8). Finally, we demonstrated that exogenous addition of PIP_2 rescues functional hyperemia, suggesting a potential therapeutic strategy for treating early impairment in SVDs. Although endothelial dysfunction is widely accepted as a central element in sporadic SVDs, it has remained elusive in CADASIL patients (4, 28). Furthermore, endothelial dysfunction has been thought to only involve impaired arteriolar dilation and blood–brain barrier (BBB) integrity (2, 3). Our findings definitively establish that functional hyperemia deficits in SVD are associated with capillary endothelial dysfunction, specifically linking a disruption in capillary-to-arteriole electrical communication to a vascular brain disorder. This endothelial dysfunction reflects diminished Kir2.1 channel activity due to reduced availability of the essential cofactor, PIP_2, and is linked to a decrease in intracellular ATP. Thus, although additional details remain to be resolved, our findings provide an outline of the complete molecular sequence of events underlying an SVD.

The current study, taken together with our previous work, demonstrates that pathogenic accumulation of TIMP3 affects two different ion channels in two different vascular cell types—K_V channels in arteriolar SMCs and Kir channels in cECs—to cause distinct K^+ channelopathy-like defects in myogenic behavior and functional hyperemia, respectively. These remarkable and unexpected findings underscore a number of important issues. First, the specific suppression of endothelial Kir2.1 channel activity in capillaries implies that, in addition to the canonical targets, SMCs and pericytes, cECs are also targets in SVD. Second, the apparent lack of a contribution of myogenic deficits (caused by up-regulation of SMC $K_V1.5$ channels) to the functional hyperemia deficits in these animals is surprising, given that myogenic responses influence how vessels respond to hyperemic stimuli. A third, related issue is the absence of an effect of Notch3^{ECD} deposits on ECs in the arteriolar compartment. A possible explanation for the continued function of Kir2.1 channels in the arteriolar endothelium of SVD mice lies in the observation that arterioles possess an internal elastic lamina, which may prevent the endothelium from being directly exposed to accumulated TIMP3 and thereby spares Kir2.1 function. This contrasts with the capillary endothelium, which shares the same basement membrane with pericytes (the presumed source of capillary Notch3^{ECD} deposits) and is thus directly exposed to the pathogenic accumulation of TIMP3 (16, 29, 30). The smooth muscle layer of arterioles, however, would be directly exposed to Notch3^{ECD} deposits and accumulated TIMP3; thus, the pathogenic consequences of this accumulation are different: inhibition of the EGFR pathway and $K_V1.5$ channel up-regulation specifically in the SMC compartment.

PIP_2 synthesis is an ATP-consuming process that depends on low-ATP–affinity PI4 and PIP5 kinases (24, 25, 27). Notably, a recent study reported a decrease in mitochondrial proteins and oxidative phosphorylation in vessels from SVD patients (31). Consistent with this latter report and the diminished PIP_2 levels reported here, we found that ATP levels were reduced in cECs freshly isolated from SVD mice compared with WT cECs. Importantly, HB-EGF, which we previously reported is able to restore functional hyperemia in SVD mice (13), also increased ATP levels and reestablished normal Kir current density in SVD cECs. As a mitogenic factor, HB-EGF has previously been shown to increase cytosolic ATP concentrations (32, 33), and expression of its cognate receptor (EGFR) in the brain vascular endothelium is high compared with that in other vascular beds (34). Despite the potential for EGFR-dependent activation of phospholipase C (35), our data and the literature support the concept that EGFR activation in SVD cECs enhances mitochondrial function, which acts presumably by increasing intracellular ATP levels to stimulate PI4/PIP5 kinase-mediated PIP_2 formation and restore normal Kir2.1 function.

Although ATP restored Kir2.1 currents, and HB-EGF elevated ATP in SVD mice, it is unlikely that intracellular ATP decreased from the low millimolar range to less than 0.5 mM to cripple PIP_2 synthesis (36). More likely, it is the ATP/ADP ratio (i.e., phosphorylation potential) that is lower in SVD cECs (37). Importantly, this decreased ATP/ADP ratio could also affect other ATP-dependent signaling cascades. A decrease in the ATP/ADP ratio in cECs could, hypothetically, increase currents through ATP-sensitive K^+ (K_{ATP}) channels. However, we didn't observe these currents in our recordings here, even in SVD conditions. ATP is also necessary for endothelial functions such as transcytosis of solutes and proteins, transporter activity, and the maintenance of ionic gradients. Although all of these activities are

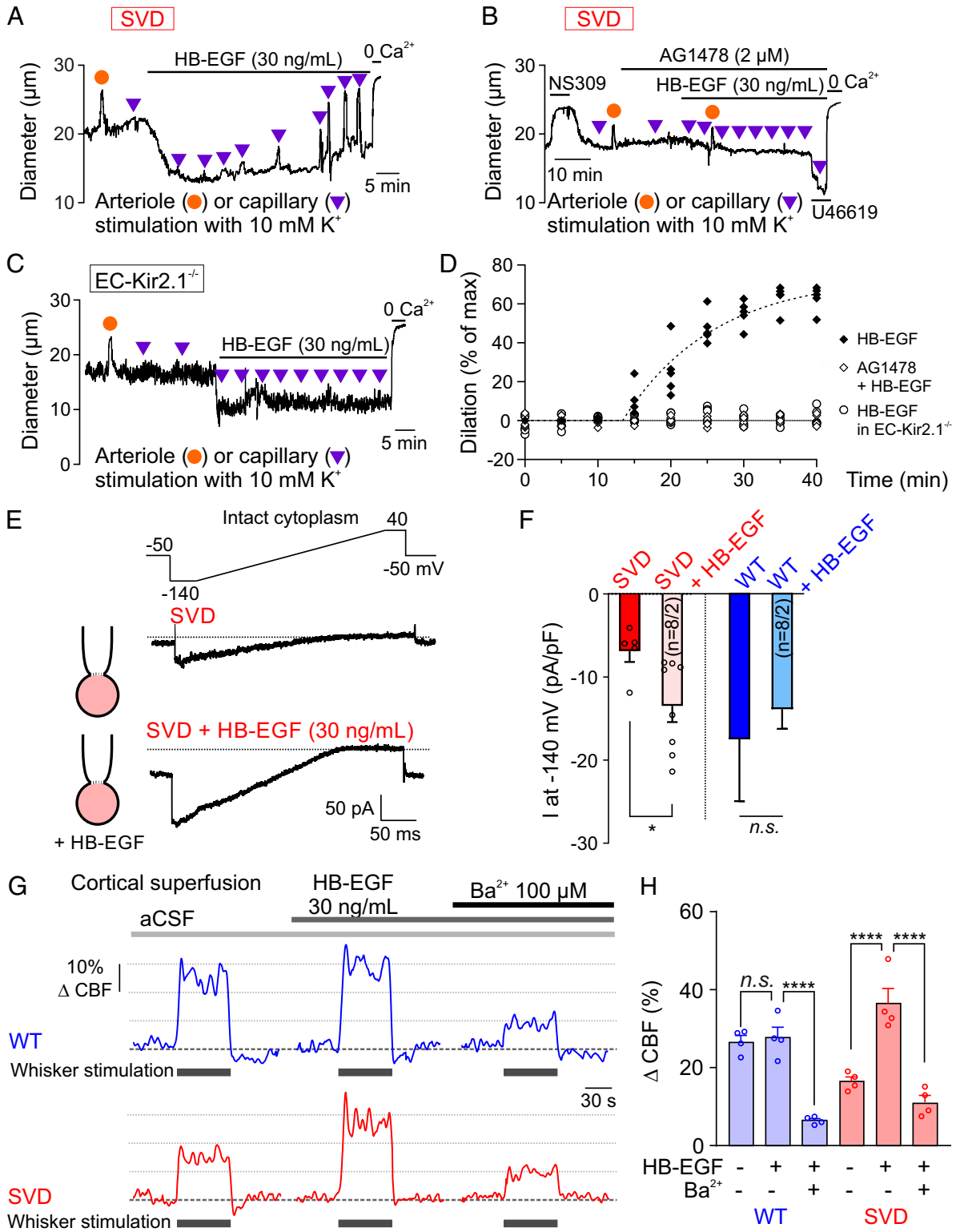

Fig. 4. Lower Kir2.1 channel currents in SVD cECs and restoration by HB-EGF. (*A* and *B*) Arteriolar diameter traces in SVD CaPA preparations showing effects of bath-applied HB-EGF on myogenic tone and upstream arteriolar dilation in the absence (*A*) and presence (*B*) of the EGFR antagonist AG1478. (*C*) Arteriolar diameter traces in CaPA preparation from an EC-Kir2.1$^{-/-}$ mouse. (*D*) Summary data showing arteriolar dilation induced by capillary stimulation with 10 mM K^+ ($n = 5$ mice per condition). (*E*) Ba^{2+}-sensitive Kir2.1 currents in freshly isolated SVD cECs, recorded in the perforated-patch configuration in the absence or presence of bath-applied HB-EGF for 20 min. (*F*) Summary data showing the effect of HB-EGF on Kir2.1 currents from SVD and WT cECs ($n = 4$–8 cECs per group from eight mice; *n.s.*, not significant; *$P < 0.05$, unpaired Student's *t* test). (*G*) Representative traces of whisker stimulation-induced changes in CBF in WT and SVD mice before and after treatment with Ba^{2+}. (*H*) Summary data showing restoration of Ba^{2+}-sensitive functional hyperemia in SVD mice by HB-EGF ($n = 4$ mice per group; *n.s.*, not significant; ****$P < 0.0001$, repeated-measures one-way ANOVA).

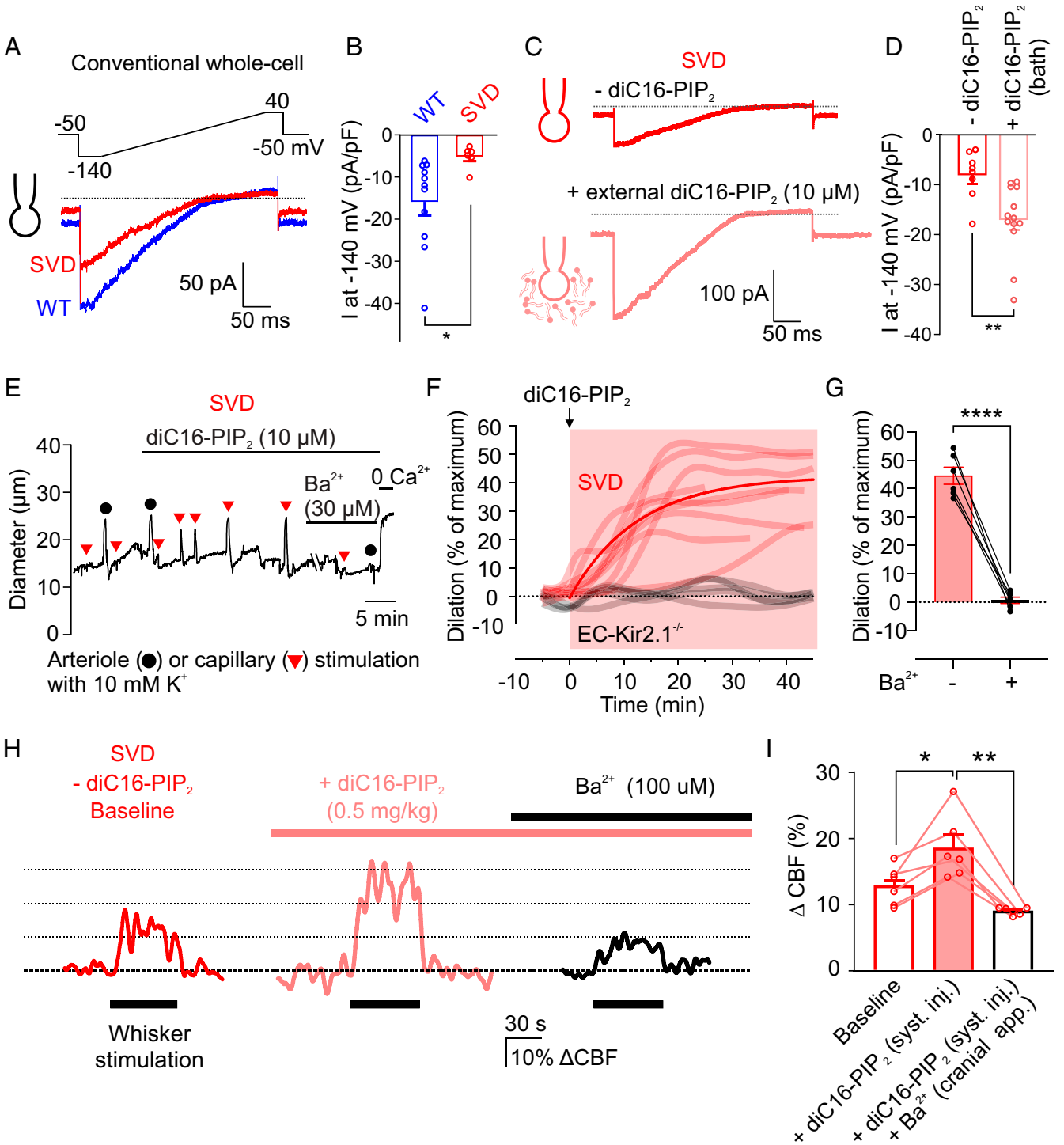

Fig. 5. Exogenous PIP_2 treatment improves functional hyperemia in SVD mice. (*A*) Kir2.1 currents recorded from WT and SVD cECs in the conventional (dialyzed cytoplasm) configuration within 3 to 5 min after gaining access (0 mM Mg-ATP in the pipette). (*B*) Summary data for Kir2.1 currents in WT and SVD cECs as in *A* ($n = 6$–11 cECs from three to four mice per group; $^*P < 0.05$, unpaired Student's *t* test). (*C* and *D*) Representative traces (*C*) and summary data (*D*) for Kir2.1 currents from SVD cECs preincubated with or without bath-applied diC16-PIP_2 for 20 min ($n = 8$–13 cECs from three mice; $^{**}P < 0.01$, unpaired Student's *t* test). (*E*) Arteriolar diameter trace showing restoration of 10 mM K^+-induced (capillary applied) dilatory responses by bath-applied diC16-PIP_2, and their inhibition by Ba^{2+}, in a CaPA preparation from an SVD mouse. (*F*) Summary data showing the effect of diC16-PIP_2 in nine SVD and five EC-Kir2.1$^{-/-}$ mice. (*G*) Summary data from six SVD mice showing elimination of K^+ (10 mM)-induced dilation by Ba^{2+} in the presence of diC16-PIP_2 ($^{****}P < 0.0001$, paired Student's *t* test). (*H*) Representative traces showing whisker stimulation-induced changes in CBF in SVD mice before and after systemic injection of diC16-PIP_2 and cortical superfusion of Ba^{2+}. (*I*) Summary data showing increased whisker stimulation-induced functional hyperemia with PIP_2 treatment and elimination by Ba^{2+} ($n = 6$ animals, $^*P < 0.05$, $^{**}P < 0.01$, repeated-measures one-way ANOVA).

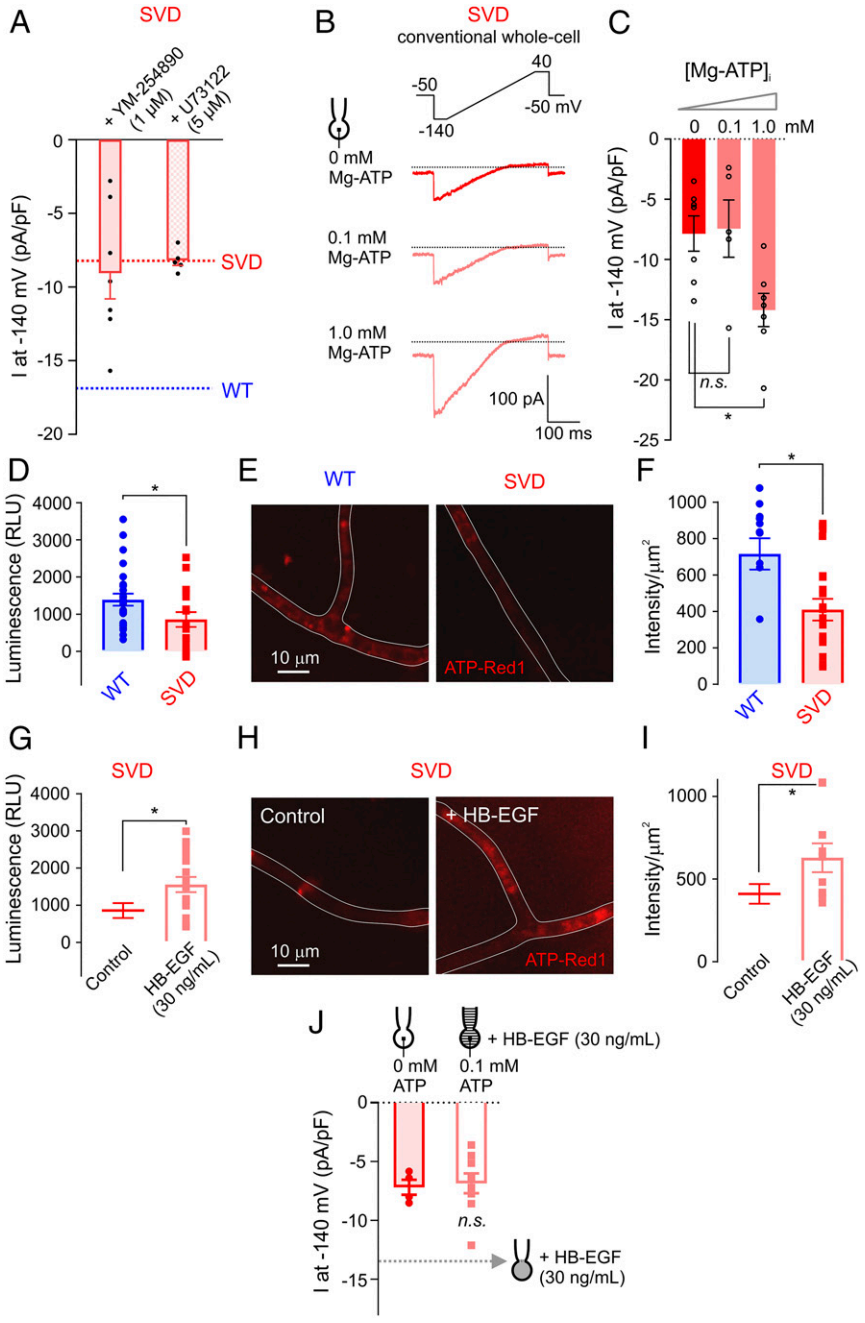

Fig. 6. Decreased intracellular ATP in capillaries from SVD mice. (*A*) Summary data for Kir2.1 currents in cECs from SVD mice measured using the perforated-patch configuration. SVD cECs were bath-incubated for ~15 min with the $G\alpha_{q/11}$ inhibitor YM-254890 or the phospholipase C inhibitor U73122 (n = 5–7 cECs from three to four mice per group). Dotted lines indicate current density observed in SVD (red) and WT (blue) cECs, as in Fig. 2*E*. (*B*) Kir2.1 currents in SVD cECs dialyzed with 0, 0.1, or 1 mM Mg-ATP in the pipette solution using the conventional configuration. (*C*) Summary data for *B* (n = 5–7 cECs from four mice; *n.s.*, not significant, *P < 0.05, one-way ANOVA). (*D–I*) Intracellular ATP levels in WT or SVD cECs, without or with HB-EGF treatment. cEC luminescence (in relative luminescence units [RLU]), reflecting luciferase-induced conversion of ATP to light, is directly proportional to cEC ATP concentration (*D* and *G*). cEC fluorescence intensity, measured with the live cell ATP dye ATP-Red1, is proportional to ATP levels (*E*, *F*, *H*, and *I*). Each data point on scatter plots in *F* and *I* represent a capillary segment, and each data point in *D* and *G* was obtained using ~500 cECs manually collected from three WT and three SVD mice (*P < 0.05, unpaired Student's t test). (*J*) Kir2.1 currents in cECs from SVD, recorded using the conventional configuration. One group of cECs was dialyzed with 0 mM Mg-ATP, and the other was dialyzed with 0.1 mM Mg-ATP and incubated with HB-EGF for ~20 min (n = 4–9 cECs from six mice; *n.s.*, not significant, unpaired Student's t test). Dotted line indicates Kir2.1 current amplitude in SVD cECs incubated with HB-EGF using the perforated configuration (as in Fig. 4*F*).

critical in controlling the BBB, there is no evidence for BBB breakdown in the SVD mouse model (14, 38), reemphasizing the concept that capillary EC metabolism remains sufficient to modulate ATP-dependent functions other than PIP_2 synthesis. In support of this, about 50% of normal capillary Kir2.1 activity was maintained at the stage of SVD investigated here, reflective of some degree of metabolic endurance. In addition to impaired PIP_2 synthesis, variabilities in subcellular PIP_2 levels in cECs could be introduced by G_qPCR signaling through localized hydrolysis (8), which could therefore stress an already limited supply and further inhibit Kir2.1-mediated signaling. The findings presented here thus represent merely the tip of the iceberg with respect to metabolic changes in ECs and their contribution to associated vascular deficits in SVD.

Because the therapeutic potential of HB-EGF is limited owing to its potent angiogenic actions and associated progression of several types of tumor (39), we instead focused on PIP_2 as an alternative therapeutic approach, demonstrating the potential of exogenously applied PIP_2 to rescue functional hyperemia deficits in SVD. Physiologically, PIP_2 is concentrated in the inner leaflet of the plasma membrane (40). Given that PIP_2 is negatively charged, we were initially surprised that it would be effective when externally applied. However, endogenous flippases and scramblases act to transport negatively charged phospholipids to the inner leaflet of the bilayer, an intrinsic process that may explain the efficacy of our approach (41). Interestingly, a loss-of-function mutation in the flippase, ATPase11B, was recently linked to endothelial dysfunction in the stroke-prone spontaneously hypertensive rat, a relevant model for sporadic SVDs (42).

Several neurovascular coupling mechanisms support functional hyperemia (7), and disrupting capillary-to-arteriole electrical signaling may alter not only the amplitude (as measured here),

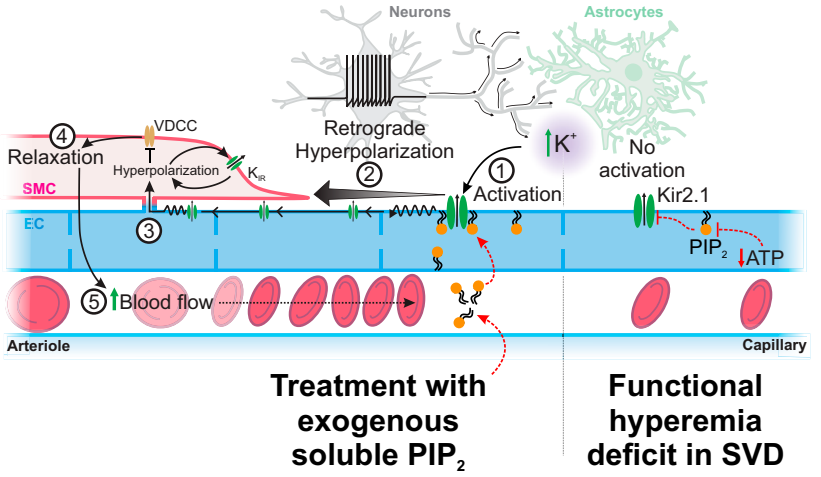

Fig. 7. Proposed mechanism by which SVDs silence Kir2.1 channel during functional hyperemia and how treatment with exogenous PIP_2 can restore the physiological response. In SVD, a substantial fraction of Kir2.1 channels in cECs are not associated with PIP_2, making them not activable by increases in extracellular K^+ from neural activity. PIP_2 treatment allows Kir2.1 channels subunits to be associated with PIP_2 and then be activable by external K^+ and hyperpolarization. This produces a regenerative hyperpolarization that spreads to adjacent ECs up to the arteriolar SMCs. Hyperpolarization then closes voltage-dependent Ca^{2+} channels (VDCCs) to cause arteriolar dilation, promoting an increase in blood flow into the capillaries.

but also the kinetics, of hyperemic responses. Whether a slower component of capillary-to-arteriole signaling, highlighted in a recent study (43), is also impacted in SVD is unknown, but a kinetic analysis of functional hyperemia in SVD would clearly extend our understanding of the pathological progression. Additionally, endothelial dysfunction could lead to consequences beyond local neurovascular uncoupling. In this context, recent analyses have revealed that entrainment of ultra-slow (~0.1 Hz) vasomotion by neural activity is critical for functional connections (6, 44). It is therefore conceivable that disruption of Kir2.1-mediated propagating hyperpolarizing signals during SVD could cripple transhemispheric coordination.

Our current results argue that fundamental alterations in extracellular matrix proteins disrupt ion channel functionalities that control vascular reactivity, and thus cerebral hemodynamics, at an early stage in SVD. We further demonstrate that the SVD-causing mutation also targets endothelial function, extending the known targets of this disease beyond SMCs and pericytes. Although ATP and PIP_2 levels in cECs from SVD mice are sufficiently reduced to have a major impact on functional hyperemia, they nonetheless appear to be high enough to sustain other ATP-dependent cellular processes. However, they likely render the capillary network more vulnerable to hypoperfusion and ischemic challenges. Thus, our data establish the foundation for a therapeutic approach for improving CBF, not only in SVD conditions, but also following ischemic stroke.

Materials and Methods

Animal Models. All experimental protocols used in this study are in accord with institutional guidelines approved by the Institutional Animal Care and Use Committee of the University of Colorado and the University of Vermont. We report this study in compliance with Animal Research: Reporting of In Vivo Experiments (ARRIVE) guidelines. The transgenic (Tg) mouse lines *TgNotch3*^{WT} (WT), *TgNotch3*^{R169C} (SVD), and double-mutant *TgNotch3*^{R169C};*Timp3*$^{+/-}$ have been previously described (14, 18). Mice (males) were used at an age of 6 mo because this is prior to the time when a significant white matter lesion burden develops and for the sake of comparison with our relevant previous studies (13, 14, 17, 19). Animals were euthanized by intraperitoneal injection of sodium pentobarbital (100 mg/kg) followed by rapid decapitation. *TgNotch3*^{WT} and *TgNotch3*^{R169C} mice (on an FVB/N background) overexpress rat WT NOTCH3 and the SVD-causing NOTCH3(R169C) mutant protein, respectively, to a similar degree (approximately fourfold) compared with the levels of endogenous NOTCH3 in non-Tg mice (WT littermates of *TgNotch3*^{WT} and *TgNotch3*^{R169C} mice) (14). Expression of SVD-causing mutations at normal endogenous levels does not produce an SVD-like phenotype, likely because the slowly developing mutant phenotype is unable to manifest during the short life span of a mouse (14). Overexpression of the mutant protein overcomes this constraint and is thus a key feature of this model. Mice carrying a germline knockout of the Kir2.1 gene specifically in ECs (i.e., EC-Kir2.1$^{-/-}$ mice) were generated by crossing mice carrying a *loxP*-flanked allele of the Kir2.1 gene *Kcnj2* (InGenious Targeting Laboratory) with mice in which Cre recombinase expression is driven by the Tek promoter (Tek-Cre; The Jackson Laboratory), as previously described and characterized (5).

cEC Isolation. Single cECs were isolated as previously described (5, 8). Briefly, cECs were obtained by mechanically disrupting two brain slices (160 μm thick each) with a Dounce homogenizer in ice-cold S1 solution (composition: 124 mM NaCl, 3 mM KCl, 2 mM $CaCl_2$, 2 mM $MgCl_2$, 1.25 mM NaH_2PO_4, 26 mM $NaHCO_3$, and 4 mM glucose) and subsequently filtered through a 62-μm nylon mesh. Retained vascular fragments were washed into dissociation solution (55 mM NaCl, 80 mM Na-glutamate, 5.6 mM KCl, 2 mM $MgCl_2$, 4 mM glucose, and 10 mM 4-(2-hydroxyethyl)-1-piperazineethanesulfonic acid [Hepes], pH 7.3), containing neutral protease (0.5 mg/mL), elastase (0.5 mg/mL; Worthington), and 100 μM $CaCl_2$, and incubated for 23 to 25 min at 37 °C. Then, collagenase type I (Worthington) was added (100 μL added to reach a final concentration of 0.5 mg/mL), and incubation continued for an additional 2 min at 37 °C. The suspension was filtered, washed, and triturated four to five times with a fire-polished glass Pasteur pipette. Cells were used within ~6 h of dispersion, and capacitances were 9.2 ± 0.3 pF (n = 15) for WT and 9.2 ± 0.7 pF (n = 16) for SVD cECs.

Arterial/Arteriolar EC Isolation. Single arterial/arteriolar ECs were obtained from mouse brains by first isolating arteries and arterioles, as previously described (5). Vessels were dissected in ice-cold solution S1 (composition indicated in *cEC Isolation*). Arterial segments were transferred to dissociation solution composed of 55 mM NaCl, 80 mM Na-glutamate, 5.6 mM KCl, 2 mM $MgCl_2$, 4 mM glucose, and 10 mM Hepes (pH 7.3), containing neutral protease (0.5 mg/mL), elastase (0.5 mg/mL; Worthington), and 100 μM $CaCl_2$, and incubated for 60 min at 37 °C. Thereafter, 0.5 mg/mL collagenase type I (Worthington) was added, and the solution was incubated for an additional 2 min at 37 °C. The vessels were then mechanically disrupted to facilitate endothelial cell liberation, vascular fragments were washed to remove enzymes, and single ECs were dispersed by triturating five times with a fire-polished glass Pasteur pipette. Cells were used within ~6 h of dispersion, and capacitances were 5.5 ± 0.5 pF (n = 8) for WT and 6.7 ± 1.3 pF (n = 10) for SVD arteriolar ECs.

Arterial/Arteriolar SMC Isolation. SMCs were isolated from intact cerebral arteries by first placing vessel segments in isolation media containing 60 mM NaCl, 80 mM Na-glutamate, 5 mM KCl, 2 mM $MgCl_2$, 10 mM glucose, and 10 mM Hepes with 1 mg/mL bovine serum albumin (BSA) (pH 7.4) at 37 °C for

10 min. Arteries were then exposed to a two-step digestion process that began with a 14-min incubation (37 °C) in media containing 0.5 mg/mL papain and 1.5 mg/mL dithioerythritol, followed by a 10-min incubation in media containing 100 μM Ca^{2+}, 0.7 mg/mL type F collagenase, and 0.4 mg/mL type H collagenase. After incubation, tissues were washed repeatedly with ice-cold isolation media and triturated with a fire-polished pipette. Liberated cells were stored on ice for use on the same day, and capacitances were 11.7 ± 1.0 pF (n = 10) for WT and 12.2 ± 1.0 pF (n = 10) for SVD SMCs.

Electrophysiology. Whole-cell currents were recorded as previously described (8) using a patch-clamp amplifier (Axopatch 200B; Molecular Devices), filtered at 1 kHz, digitized at 5 kHz, and analyzed with Clampfit 10.3 software. Recordings were performed in the conventional or perforated whole-cell configuration. Bath solution was 80 mM NaCl, 60 mM KCl, 1 mM $MgCl_2$, 10 mM Hepes, 4 mM glucose, and 2 mM $CaCl_2$ (pH 7.4). In the conventional whole-cell configuration, pipette solution was composed of 10 mM NaOH, 11.4 mM KOH, 128.6 mM KCl, 1.1 mM $MgCl_2$, 2.2 mM $CaCl_2$, 5 mM ethylene glycol-bis(β-aminoethyl ether)-*N*,*N*,*N*′,*N*′-tetraacetic acid (EGTA), and 10 mM Hepes (pH 7.2). As noted in *Results*, the pipette solution was supplemented in some experiments with ATP (0.1 or 1 mM) or an analog of PIP_2. In the perforated-patch configuration, the pipette solution consisted of 10 mM NaCl, 26.6 mM KCl, 110 mM K^+ aspartate, 1 mM $MgCl_2$, 10 mM Hepes, and 200 to 250 μg/mL amphotericin B, added freshly on the day of the experiment.

ATP Measurements in Brain Capillaries.

Luciferase-based ATP assay. ATP in brain capillaries was measured by quantifying the luminescence emitted by the luciferase reaction of luciferin with ATP using a luminescent ATP detection assay kit (700410; Cayman Chemicals). First, brain capillary networks were isolated from mouse brains by mechanical disruption (homogenization) of 160-μm–thick brain slices in solution S1 (composition indicated in *cEC Isolation*). The brain homogenate was passed through a 62-μm mesh filter, and retained capillaries were subsequently washed into phosphate-buffered saline (PBS) and placed in the collection chamber. Pipettes with large tips, made by pulling borosilicate glass and fire-polishing to smooth glass edges, were used for collection. Approximately 500 cECs were manually collected in each reaction (data point) by carefully applying suction while avoiding aspirating noncapillary cells. Collected cells were lysed by sonication in detection sample buffer and then frozen at −20 °C until the assay was finished (24 to 48 h). Subsequent assay steps were performed according to the manufacturer's instructions. Luminescence from luciferase activity was measured and recorded using a Synergy H plate reader, and the relative luminescence was corrected by blank subtraction. Luminescence per 1,000 cells was calculated and plotted.

ATP-Red1 live-cell dye. ATP levels in brain capillaries were also assessed using BioTracker ATP-Red1 (SCT045; Millipore Sigma), a live-cell, red fluorescent imaging probe for ATP, as described by the manufacturer. Briefly, brain capillary segments were isolated by mechanical disruption without enzymatic digestion and subsequently incubated with 10 μM ATP-Red1 at 37 °C for 15 min. Capillaries were washed with PBS and then imaged using a Nikon C2 confocal microscope using exactly the same acquisition conditions for all samples. Fluorescence intensity per surface area was calculated using ImageJ.

Ex Vivo CaPA Preparation. The CaPA preparation was obtained as previously described (5, 45) by dissecting intracerebral arterioles arising from the M1 region of the middle cerebral artery, leaving the attached capillary bed intact. Precapillary arteriolar segments were cannulated on glass micropipettes with one end occluded by a tie and pressurized using a Living Systems Instrumentation pressure servo controller with a mini peristaltic pump. The ends of the capillaries were then sealed by the downward pressure of an overlying glass micropipette. CaPA preparations were superfused (4 mL/min) with prewarmed (36 ± 1 °C), gassed (5% CO_2, 20% O_2, 75% N_2) artificial cerebrospinal fluid (aCSF) for at least 30 min.

The composition of aCSF was 125 mM NaCl, 3 mM KCl, 26 mM $NaHCO_3$, 1.25 mM NaH_2PO_4, 1 mM $MgCl_2$, 4 mM glucose, 2 mM $CaCl_2$, pH 7.3 (with aeration with 5% CO_2). Application of pressure (40 mmHg) to the cannulated parenchymal arteriole segment in this preparation pressurized the entire tree and induced myogenic tone in the arteriolar segment. Only viable CaPA preparations, defined as those that developed pressure-induced myogenic tone greater than 15%, were used in subsequent experiments. Arteriolar viability was validated by bath-applying NS309 (1 μM), which causes an endothelial-dependent vasodilation through activation of small and intermediate conductance, Ca^{2+}-sensitive K^+ (SK and IK, respectively) channels, or the thromboxane receptor agonist U46619, which causes robust vasoconstriction (*SI Appendix*, Figs. S1 and S6). Drugs were applied by addition to the superfusate. Dilatory responses of the attached arteriole segment to K^+ were obtained by applying 10 mM K^+ onto capillary extremities by pressure ejection from a glass micropipette (tip diameter, ∼5 μm) attached to a Picospritzer III (Parker) at ∼5 psi for 20 s. In some control experiments, K^+ was applied directly to the arteriole segment. The luminal diameter of the parenchymal arteriole was acquired in two regions at 15 Hz using a charge-coupled device (CCD) camera and IonWizard 6.2 edge-detection software (IonOptix). Changes in arteriolar diameter were calculated from the average luminal diameter measured over the last 10 s of stimulation and were normalized to the maximum dilatory responses in 0 mM Ca^{2+} bath solution at the end of each experiment using the following equation: [(change in diameter)/(maximal diameter-initial diameter)] × 100.

FRAP Measurements. The organ chamber was placed on the stage of a Nikon Ti-E Inverted C2 Confocal Microscope equipped with a plan apo 40× Oil differential interference contrast (DIC) H objective. CaPA preparations were loaded with 10 μM 1,1′-dioctadecyl-3,3,3′,3′-tetramethylindodicarbocyanine perchlorate ($DiIC_{18}$) (Invitrogen) or 10 μM soluble BODIPY PIP_2 (Echelon Biosciences) for 20 min in circulating, prewarmed (36 ± 1 °C), gassed (5% CO_2, 20% O_2, 75% N_2) aCSF, followed by a 20-min wash. Fluorescence was monitored (488 nm excitation wavelength) at low laser power (<3%). A circular region, 3 μm in diameter, was bleached at high laser power (>70%) for 2 s using the NIS-Element software FRAP protocol. Fluorescence recovery curves were obtained by normalizing the fluorescence intensity using the equation, $I = [(I_t - I_{min})/(I_{max} - I_{min})] \times 100$, where I is the normalized intensity, I_t is the intensity at a given time point, I_{min} is the minimum intensity after photobleaching, and I_{max} is the mean intensity before photobleaching. Diffusion coefficients were calculated using the simFRAP ImageJ plugin developed by Blumenthal et al. (46).

In Vivo Imaging of Cerebral Hemodynamics. Mice were initially anesthetized with isoflurane (5% induction, 2% maintenance) during the surgical procedure as previously described (5, 8). Upon obtaining surgical-level anesthesia, the skull was exposed and cleaned, and a stainless-steel head plate was attached over the left hemisphere using dental cement and superglue. During experimental recording, isoflurane anesthesia was replaced with α-chloralose (50 mg/kg) and urethane (750 mg/kg). FITC-dextran (2,000 kDa) was systemically injected to visualize the cerebral vasculature and for contrast imaging of RBCs. The direction of RBCs flowing into the brain was used to identify penetrating arterioles, and the downstream capillaries were selected for study. A pipette was then maneuvered to the proximity of a capillary under study, and aCSF containing 10 mM K^+ was ejected (200 to 300 ms, 8 ± 1 psi, ∼4 pL) directly onto the capillary. The ejected volume was monitored by the inclusion of tetramethylrhodamine isothiocyanate (TRITC)-labeled (150 kDa) dextran (Fig. 1*E*). RBC flux data were collected using 5-kHz line scanning. All recordings were acquired using a multiphoton laser-scanning microscope (Zeiss LSM-7; Zeiss) coupled to a Coherent Chameleon Vision II Titanium-Sapphire pulsed infrared laser (Coherent) and equipped with a 20× objective (Plan Apochromat 1.0 numerical aperture [N.A.] DIC visible infrared [VIS-IR] water-immersion). Excitation of FITC and TRITC was at 820 nm, and the emission fluorescence was separated using 500- to 550-nm and 570- to 610-nm bandpass filters, respectively.

Measurement of Functional Hyperemia In Vivo. Functional hyperemia induced by whisker stimulation was measured in the mouse somatosensory cortex using LDF as described previously (5), with some modifications. Briefly, after first anesthetizing mice with isoflurane (5% induction, 2% maintenance), a catheter was inserted into the femoral artery for monitoring blood pressure and collecting blood samples for blood gas analysis. A cranial window was made over the somatosensory cortex, superfused with aerated, warm (∼37 °C) aCSF. Cortical CBF was recorded through the cranial window with a laser Doppler probe (PeriMed) under the combined anesthesia of α-chloralose (50 mg/kg) and urethane (750 mg/kg). Functional hyperemic responses are presented as the percent change in CBF induced by stroking the contralateral vibrissae at a frequency of ∼3 Hz for 1 min (i.e., whisker stimulation) relative to baseline values. Pharmacological agents were topically applied by adding to the cortical superfusate, with the exception of diC16-PIP_2, which was systemically administered via the catheter inserted into the femoral artery. During CBF measurements, blood pressure was continuously recorded via the femoral artery cannula, and body temperature was maintained at 37 °C using a servo-controlled heating pad with a rectal temperature sensor probe. All data were recorded and analyzed using LabChart software (AD Instruments).

NEUROSCIENCE

Reagents. BODIPY-labeled soluble PIP_2 was purchased from Echelon Biosciences; diC8-PIP_2 and diC16-PIP_2 were purchased from Cayman Chemical; human bioactive ADAM17 was purchased from R&D Systems; NS309 and U46619 were purchased from Tocris Bioscience; and recombinant human TIMP3 was purchased from RayBiotech. All other chemicals and reagents were obtained from Sigma-Aldrich.

Statistical Analysis. Data in figures and text are presented as means ± SEM. Statistical testing was performed using GraphPad Prism 8 software. All data passed the Kolmogorov–Smirnov test for normality. Statistical significance was determined using either two-tailed Student's *t* test or one-way ANOVA, followed by Tukey's post hoc test, unless otherwise stated.

Data Availability. All study data are included in the article and/or supporting information.

ACKNOWLEDGMENTS. We thank Reem Aboushousha for assistance with the luciferase-based ATP assay. This study was supported by Postdoctoral Fellowship 17POST33650030 (to O.F.H.), Career Development Award 20CDA35310097 (to O.F.H.), Scientist Development Grants 14SDG20150027 (to M.K.) and 17SDG33670237 (to T.A.L.) from the American Heart Association, a Career Development Award from the Cardiovascular Research Institute at the University of Vermont (to O.F.H.), awards from the CADASIL Together We Have Hope nonprofit organization (to F.D. and M.T.N.), the Totman Medical Research Trust (M.T.N.), a grant from the Center for Women's Health Research located at the University of Colorado Anschutz Medical Campus (to F.D.), research grants from the University of Pennsylvania Orphan Disease Center in partnership with the cureCADASIL (to F.D. and M.K.), the Fondation Leducq Transatlantic Network of Excellence on the Pathogenesis of Small Vessel Disease of the Brain (A.J. and M.T.N.), the European Union Horizon 2020 Research and Innovation Program SVDs@target under Grant Agreement 666881 (to A.J. and M.T.N.), French National Agency of Research Grant ANR-16-RHUS-0004 (to A.J.), grants from the National Institute of Neurological Disorders and Stroke and National Institute of Aging under Grant R01-NS-110656 (to M.T.N.), National Institute of Diabetes and Digestive and Kidney Diseases Grant R37-DK-053832 (to M.T.N.), and National Institute of General Medical Sciences Grant (P20-GM-135007; Principle Investigators Mary Cushman and Mark Nelson, Vermont Center for Cardiovascular and Brain Health [to M.K. and O.F.H.]); and National Heart, Lung, and Blood Institute Grants R01-HL-136636 (to F.D.) and P01-HL-095488, R01-HL-121706, 7UM- HL-1207704, R01-HL-131181, and R35-HL-140027 (to M.T.N.).

1. L. Pantoni, Cerebral small vessel disease: From pathogenesis and clinical characteristics to therapeutic challenges. *Lancet Neurol.* **9**, 689–701 (2010).
2. J. M. Wardlaw, C. Smith, M. Dichgans, Small vessel disease: Mechanisms and clinical implications. *Lancet Neurol.* **18**, 684–696 (2019).
3. C. Iadecola *et al*., Vascular cognitive impairment and dementia: JACC scientific expert panel. *J. Am. Coll. Cardiol.* **73**, 3326–3344 (2019).
4. H. Chabriat, A. Joutel, M. Dichgans, E. Tournier-Lasserve, M.-G. Bousser, Cadasil. *Lancet Neurol.* **8**, 643–653 (2009).
5. T. A. Longden *et al*., Capillary K^+-sensing initiates retrograde hyperpolarization to increase local cerebral blood flow. *Nat. Neurosci.* **20**, 717–726 (2017).
6. P. J. Drew, C. Matéo, K. L. Turner, X. Yu, D. Kleinfeld, Ultra-slow oscillations in fMRI and resting-state connectivity: Neuronal and vascular contributions and technical confounds. *Neuron* **107**, 782–804 (2020).
7. L. Kaplan, B. W. Chow, C. Gu, Neuronal regulation of the blood-brain barrier and neurovascular coupling. *Nat. Rev. Neurosci.* **21**, 416–432 (2020).
8. O. F. Harraz, T. A. Longden, F. Dabertrand, D. Hill-Eubanks, M. T. Nelson, Endothelial GqPCR activity controls capillary electrical signaling and brain blood flow through PIP_2 depletion. *Proc. Natl. Acad. Sci. U.S.A.* **115**, E3569–E3577 (2018).
9. A. Moshkforoush *et al*., The capillary Kir channel as sensor and amplifier of neuronal signals: Modeling insights on K^+-mediated neurovascular communication. *Proc. Natl. Acad. Sci. U.S.A.* **117**, 16626–16637 (2020).
10. O. F. Harraz, D. Hill-Eubanks, M. T. Nelson, PIP_2: A critical regulator of vascular ion channels hiding in plain sight. *Proc. Natl. Acad. Sci. U.S.A.* **117**, 20378–20389 (2020).
11. C. L. Huang, S. Feng, D. W. Hilgemann, Direct activation of inward rectifier potassium channels by PIP_2 and its stabilization by Gbetagamma. *Nature* **391**, 803–806 (1998).
12. S. B. Hansen, X. Tao, R. MacKinnon, Structural basis of PIP_2 activation of the classical inward rectifier K^+ channel Kir2.2. *Nature* **477**, 495–498 (2011).
13. C. Capone *et al*., Mechanistic insights into a TIMP3-sensitive pathway constitutively engaged in the regulation of cerebral hemodynamics. *eLife* **5**, e17536 (2016).
14. A. Joutel *et al*., Cerebrovascular dysfunction and microcirculation rarefaction precede white matter lesions in a mouse genetic model of cerebral ischemic small vessel disease. *J. Clin. Invest.* **120**, 433–445 (2010).
15. C. Huneau *et al*., Altered dynamics of neurovascular coupling in CADASIL. *Ann. Clin. Transl. Neurol.* **5**, 788–802 (2018).
16. M. Monet-Leprêtre *et al*., Abnormal recruitment of extracellular matrix proteins by excess Notch3 ECD: A new pathomechanism in CADASIL. *Brain* **136**, 1830–1845 (2013).
17. F. Dabertrand *et al*., Potassium channelopathy-like defect underlies early-stage cerebrovascular dysfunction in a genetic model of small vessel disease. *Proc. Natl. Acad. Sci. U.S.A.* **112**, E796–E805 (2015).
18. C. Capone *et al*., Reducing Timp3 or vitronectin ameliorates disease manifestations in CADASIL mice. *Ann. Neurol.* **79**, 387–403 (2016).
19. J. T. Fontaine, A. C. Rosehart, A. Joutel, F. Dabertrand, HB-EGF depolarizes hippocampal arterioles to restore myogenic tone in a genetic model of small vessel disease. *Mech. Ageing Dev.* **192**, 111389 (2020).
20. M. Koide *et al*., The yin and yang of KV channels in cerebral small vessel pathologies. *Microcirculation* **25**, e12436 (2018).
21. J. M. Quayle, J. G. McCarron, J. E. Brayden, M. T. Nelson, Inward rectifier K^+ currents in smooth muscle cells from rat resistance-sized cerebral arteries. *Am. J. Physiol.* **265**, C1363–C1370 (1993).
22. T. A. Longden, M. T. Nelson, Vascular inward rectifier K^+ channels as external K^+ sensors in the control of cerebral blood flow. *Microcirculation* **22**, 183–196 (2015).
23. D. A. Fruman, R. E. Meyers, L. C. Cantley, Phosphoinositide kinases. *Annu. Rev. Biochem.* **67**, 481–507 (1998).
24. T. Gehrmann *et al*., Functional expression and characterisation of a new human phosphatidylinositol 4-kinase PI4K230. *Biochim. Biophys. Acta* **1437**, 341–356 (1999).
25. S. Suer, A. Sickmann, H. E. Meyer, F. W. Herberg, L. M. Heilmeyer Jr., Human phosphatidylinositol 4-kinase isoform PI4K92. Expression of the recombinant enzyme and determination of multiple phosphorylation sites. *Eur. J. Biochem.* **268**, 2099–2106 (2001).
26. Z. A. Knight, K. M. Shokat, Features of selective kinase inhibitors. *Chem. Biol.* **12**, 621–637 (2005).
27. A. Balla, T. Balla, Phosphatidylinositol 4-kinases: Old enzymes with emerging functions. *Trends Cell Biol.* **16**, 351–361 (2006).
28. I. de Boer *et al*., RVCL-S and CADASIL display distinct impaired vascular function. *Neurology* **91**, e956–e963 (2018).
29. A. Armulik *et al*., Pericytes regulate the blood-brain barrier. *Nature* **468**, 557–561 (2010).
30. M. S. Thomsen, L. J. Routhe, T. Moos, The vascular basement membrane in the healthy and pathological brain. *J. Cereb. Blood Flow Metab.* **37**, 3300–3317 (2017).
31. A. Zellner *et al*., CADASIL brain vessels show a HTRA1 loss-of-function profile. *Acta Neuropathol.* **136**, 111–125 (2018).
32. P. R. Nagareddy *et al*., Maintenance of adrenergic vascular tone by MMP transactivation of the EGFR requires PI3K and mitochondrial ATP synthesis. *Cardiovasc. Res.* **84**, 368–377 (2009).
33. R. Pandey *et al*., Estrogen deficiency induces memory loss via altered hippocampal HB-EGF and autophagy. *J. Endocrinol.* **244**, 53–70 (2020).
34. A. Jambusaria *et al*., Endothelial heterogeneity across distinct vascular beds during homeostasis and inflammation. *eLife* **9**, 1117–1132 (2020).
35. Z. Xie *et al*., Phospholipase C-gamma1 is required for the epidermal growth factor receptor-induced squamous cell carcinoma cell mitogenesis. *Biochem. Biophys. Res. Commun.* **397**, 296–300 (2010).
36. T. W. Traut, Physiological concentrations of purines and pyrimidines. *Mol. Cell. Biochem.* **140**, 1–22 (1994).
37. C. M. Metallo, M. G. Vander Heiden, Understanding metabolic regulation and its influence on cell physiology. *Mol. Cell* **49**, 388–398 (2013).
38. R. M. Rajani *et al*., Blood brain barrier leakage is not a consistent feature of white matter lesions in CADASIL. *Acta Neuropathol. Commun.* **7**, 187 (2019).
39. P. P. Ongusaha *et al*., HB-EGF is a potent inducer of tumor growth and angiogenesis. *Cancer Res.* **64**, 5283–5290 (2004).
40. B. Hille, E. J. Dickson, M. Kruse, O. Vivas, B.-C. Suh, Phosphoinositides regulate ion channels. *Biochim. Biophys. Acta* **1851**, 844–856 (2015).
41. Y. Yang, M. Lee, G. D. Fairn, Phospholipid subcellular localization and dynamics. *J. Biol. Chem.* **293**, 6230–6240 (2018).
42. R. M. Rajani *et al*., Reversal of endothelial dysfunction reduces white matter vulnerability in cerebral small vessel disease in rats. *Sci. Transl. Med.* **10**, eaam9507 (2018).
43. P. Thakore *et al*., Brain endothelial cell TRPA1 channels initiate neurovascular coupling. *eLife* **10**, 63040 (2021).
44. C. Matéo, P. M. Knutsen, P. S. Tsai, A. Y. Shih, D. Kleinfeld, Entrainment of arteriole vasomotor fluctuations by neural activity is a basis of blood-oxygenation-level-dependent, "Resting-State" connectivity. *Neuron* **96**, 936–948.e3 (2017).
45. A. C. Rosehart, A. C. Johnson, F. Dabertrand, Ex vivo pressurized hippocampal capillary-parenchymal arteriole preparation for functional study. *J. Vis. Exp.* **154**, e60676 (2019).
46. D. Blumenthal, L. Goldstien, M. Edidin, L. A. Gheber, Universal approach to FRAP analysis of arbitrary bleaching patterns. *Sci. Rep.* **5**, 11655 (2015).